Short communication

Optimizing Li/MnO$_2$ batteries: Relating manganese dioxide properties and electrochemical performance

Wesley M. Dose, Scott W. Donne*

Discipline of Chemistry, University of Newcastle, Callaghan, NSW 2308, Australia

HIGHLIGHTS

► We have considered the optimization of MnO$_2$ for non-aqueous Li/MnO$_2$ batteries.
► Electrochemical performance is related directly to the heat treated MnO$_2$ properties.
► Materials are optimized by different material properties depending on discharge rate.
► Results aid intelligent design of cathodes for high performance lithium batteries.

ARTICLE INFO

ABSTRACT

The electrochemical performance of heat treated manganese dioxide in lithium batteries is for the first time directly related to the numerous physical properties which characterize this battery material. The effect of discharge rate on these relationships is also investigated. Three of these properties are considered, revealing that at low discharge rates heat treated manganese dioxide is optimized by a pyrolusite fraction of ~0.65, high Mn(IV), and low surface area; while at high discharge rates slightly higher pyrolusite content (~0.73), high Mn(IV), and surface area around 44 m^2 g^{-1} are most beneficial. The relationships described here will assist in directing the synthesis and preparative treatment of manganese dioxides for higher performing lithium batteries.

1. Introduction

The majority of portable consumer batteries produced worldwide use manganese dioxide as the cathode material. Since the 1980s non-aqueous Li/MnO$_2$ battery systems have found popular application in high energy density and high power consumer electronics [1]. The Li/MnO$_2$ battery system has many advantages over its counterparts, most commonly lithium cobalt oxides or lithium nickel oxides. Based on cost and abundance, manganese dioxide is a much more viable material in supporting growing consumer power demands. Additionally, manganese dioxide is a much safer material to use in these cells, while also providing reasonable electrochemical output [2]. The material of choice for these cells is electrolytic manganese dioxide (EMD) which is heated (usually between 250 and 400 °C) prior to use to remove problematic water content and create a structure which is thought to be more suitable to lithium intercalation [3–5].

Despite widespread use of manganese dioxide in lithium batteries, the effects of numerous material properties on the electrochemical performance was previously unknown, making the selection and treatment of materials for superior performance essentially empirical in nature. We report here what is to our knowledge the first detailed report linking the numerous material properties which characterize heat treated EMD (HEMD) to its electrochemical performance in Li/MnO$_2$ batteries.

2. Experimental

The details of the synthesis of the EMD materials used in this work have been described previously [6]. Essentially it is based on the anodic electrolysis (20–100 A m^{-2}) of an acidic (~0.3 M H$_2$SO$_4$) solution of MnSO$_4$ (~1.0 M) at elevated temperature (90–99 °C). After deposition the solid EMD was mechanically stripped from the substrate (titanium), washed thoroughly to neutralize any

* Corresponding author. Tel.: +61 2 4921 5477; fax: +61 2 4921 5472.
E-mail address: scott.donne@newcastle.edu.au (S.W. Donne).

entrained electrolyte, and then milled to a sub105 μm powder. Five different EMD samples were used as the starting materials in this work.

The method of kinetic analysis, based on thermogravimetric (TG) experiments, to determine the necessary isothermal heating time to remove the problematic water content from the EMD structure has been outlined in detail in our earlier work [7]. These heat treatment regimes were carried out by heating ∼10 g of EMD in an alumina crucible in a Eurotherm HTC1400 furnace with a static air atmosphere. The properties of each material generated were characterized by X-ray diffraction to determine structure, BET surface analysis to determine morphology, and potentiometric titration to determine chemical composition (see Ref. [8] for methods). Electrochemical properties of the samples were measured using CR2032 coin-type cells assembled in a dry argon filled glove box. The working electrode was fabricated by compressing a 1:8:1 mixture (by weight) of EMD:graphite:binder (polyvinylidene fluoride) into a pellet 1 cm in diameter and ∼1 mm thick, which was subsequently dried at 110 °C under vacuum for 12 h. Lithium foil served as the anode, while a Celgard 2400 sheet was employed as a separator. The electrolyte was a solution of 1 M LiPF$_6$ in 1:1 w/w ethylene carbonate:dimethyl carbonate. Using galvanostatic mode, the cells were tested by a Perkin Elmer VMP2 multi-channel potentiostat at room temperature.

3. Results and discussion

Data summarizing the structure, composition and morphology of the five prepared EMD samples, and the 23 HEMD materials derived from these, were determined and are shown in Table 1. We note here, however, that as expected, there exists considerable variation between the HEMD properties, not only with respect to heating temperature, but also depending on the properties of the starting EMD.

The primary capacity for each material at discharge rates of 2, 5, 10 and 20 mA g^{-1} of MnO$_2$ with a cut-off voltage of 2.0 V, was used as the indicator for electrochemical performance (these data are listed in Table 2). The average capacity for unheated EMD was about half that of HEMD (34% and 70% utilization, respectively, at 2 mA g^{-1}), indicating a different failure mechanism between these cells. Therefore, the EMD materials were excluded from our subsequent analysis. Considerable variation in performance is evident between the HEMD materials, with capacities ranging from 113 to 265 mAh g^{-1} (37–86% utilization) at the 2 mA g^{-1} rate. The differences in electrochemical performance can be attributed to the structure, composition and morphological characteristics of these materials. To relate these, a statistical model was employed, which involved fitting the expression in Eq. (1) for each discharge rate to ascertain how the contribution to performance varied with discharge rate for a given parameter. In this expression, a_0 is

Table 1
Material properties of starting EMD and heat treated EMD samples.

| | Synthesis | | | | | | | | |
	T (°C)[a]	Time (h)	P_r[b]	UCV (Å^3)[c]	t (Å)[d]	Mn(IV) (%)	Mn(III) (%)	CVF[e]	BET SA (m^2 g^{-1})[f]
M1	25	–	0.39	119.4	221.2	56.3	3.07	0.069	19.0
	200	13.12	0.45	117.7	208.5	57.3	3.99	0.040	19.8
	250	12.38	0.49	117.3	206.0	60.0	2.43	0.026	18.8
	300	7.15	0.78	115.0	169.7	54.9	5.60	0.001	18.3
	350	1.48	0.80	114.3	187.4	54.0	6.21	0.000	14.7
	400	–	–	–	–	–	–	–	–
M2	25	–	0.39	119.9	168.9	53.4	5.58	0.075	45.4
	200	22.62	0.66	117.7	152.8	51.2	6.28	0.044	42.7
	250	13.97	0.73	116.8	166.4	53.9	8.97	0.014	44.3
	300	3.53	0.74	115.9	173.5	54.5	6.97	0.015	39.1
	350	0.33	0.73	115.9	171.1	53.2	9.20	0.000	42.9
	400	–	–	–	–	–	–	–	–
M3	25	–	0.43	118.5	172.8	57.6	2.14	0.087	43.1
	200	25.33	0.65	116.3	169.7	56.5	2.67	0.052	42.8
	250	12.95	0.71	114.8	141.5	60.5	0.81	0.048	39.5
	300	4.68	0.73	114.8	159.5	53.6	0.82	0.041	44.6
	350	1.65	0.76	114.2	175.8	56.6	4.18	0.016	39.0
	400	0.60	0.77	113.4	199.8	56.7	4.43	0.000	39.2
M4	25	–	0.35	120.0	141.6	59.0	0.05	0.100	66.1
	200	14.33	0.65	118.2	124.0	58.0	0.95	0.061	68.6
	250	7.12	0.72	116.4	162.8	59.7	2.74	0.043	67.3
	300	3.68	0.70	115.9	114.1	57.9	3.18	0.030	62.7
	350	2.02	0.75	114.2	141.0	58.2	3.34	0.025	57.6
	400	0.68	0.76	113.4	142.6	57.2	3.91	0.028	58.4
M5	25	–	0.41	120.0	153.6	58.6	1.85	0.082	31.0
	200	25.90	0.64	117.3	174.6	61.2	0.13	0.058	24.9
	250	21.38	0.69	116.8	158.2	61.0	0.09	0.038	24.8
	300	5.90	0.76	115.5	141.4	61.7	0.63	0.025	21.6
	350	1.50	0.81	113.5	232.3	59.8	1.48	0.011	20.9
	400	0.53	0.80	113.5	229.0	59.7	1.89	0.019	24.9

[a] T: Heating temperature used for thermal synthesis.
[b] P_r: Pyrolusite fraction.
[c] UCV: Unit cell volume.
[d] t: Average crystallite size.
[e] CVF: Cation vacancy fraction.
[f] BET SA: BET surface area.

Table 2
Electrochemical performance of starting EMD and heat treated EMD samples.

	Temperature (°C)	Primary capacity (mAh g^{-1})			
		2 mA g^{-1}	5 mA g^{-1}	10 mA g^{-1}	20 mA g^{-1}
M1	25	81.1	62.0	42.6	40.2
	200	112.5	99.0	59.4	33.2
	250	189.0	161.7	98.3	79.6
	300	212.6	214.4	142.0	145.0
	350	211.4	203.3	149.7	116.5
	400	–	–	–	–
M2	25	110.8	91.1	84.2	74.0
	200	199.5	187.3	198.7	171.1
	250	243.1	222.8	220.8	198.5
	300	235.2	226.0	234.6	218.2
	350	234.4	223.6	231.4	223.2
	400	–	–	–	–
M3	25	72.1	66.9	56.5	48.0
	200	155.6	139.6	89.1	97.3
	250	213.1	211.9	202.3	180.2
	300	217.3	216.5	206.2	179.0
	350	204.9	201.7	167.2	179.0
	400	204.8	217.1	202.9	207.8
M4	25	88.4	82.2	70.9	58.5
	200	164.6	159.6	130.4	107.3
	250	217.3	188.1	183.8	152.4
	300	224.7	213.6	208.3	180.2
	350	234.4	231.5	221.9	196.8
	400	235.6	218.6	227.0	209.0
M5	25	177.2	135.5	99.8	93.1
	200	251.5	253.3	240.1	202.8
	250	265.1	251.0	243.4	239.9
	300	258.5	256.3	244.2	223.8
	350	245.3	251.9	246.8	219.2
	400	248.6	265.8	248.5	220.3

a constant, a_i are a series of coefficients describing the extent of contribution of the variable x_i to the performance.

$$\text{Performance} = a_0 + \sum_{i=1}^{n}\left(a_{i_1}x_i + a_{i_2}x_i^2\right) \qquad (1)$$

The goodness-of-fit for this expression was determined from the r^2 value. To represent the materials, the variables (x_i) used were: pyrolusite content (P_r), unit cell volume, average crystallite size, Mn(IV) percentage, Mn(III) percentage, cation vacancy fraction, and BET surface area. Prior to use in our model, the variables were normalized to be between −1 and 1. Using this model, a good fit between the calculated performance and the experimental data was achieved in all cases (r^2 values of 0.90 ± 0.03).

The individual contribution of a variable (x_i) to the performance at a given discharge rate was then isolated by taking the sum of the related terms from Eq. (1), i.e.

$$\text{Performance} = a_{i_1}x_i + a_{i_2}x_i^2 \qquad (2)$$

where the symbols here have the same meaning as in Eq. (1). Plotting the performance term generated by this equation against the measured variable allowed us to isolate the effect of this variable on the electrochemical performance. It follows then that combining all the relationships found in this study should point to the properties of HEMD which will exhibit optimum capacity. It should be recognized, however, that this ideal combination may be intrinsically impossible due to the fact that both the EMD synthesis conditions and the heat treatment conditions affect the properties of the final HEMD product in such a way as to inevitably link some of the material properties [9,10]. For instance, high deposition

current leads to an EMD which is more disordered, with smaller crystallites and high BET surface area [9], making a material with both high crystallinity and BET surface area an unlikely prospect.

The following discussion focuses on the effect on performance of three key variables: pyrolusite content, Mn(IV) fraction and surface area, which are key factors in characterizing the HEMD structure, composition and morphology, respectively. Fig. 1 shows the effect of the pyrolusite content (P_r) on electrochemical performance. This parameter has a large influence on the performance, more than twice that of other parameters at the 2 and 5 mA g^{-1} discharge rates and is at least equally significant for the 10 and 20 mA g^{-1}. The spread of contribution to performance is also much greater at lower rates. This reveals that material structure is a more critical feature for slower discharge.

For a given discharge rate there is an optimum pyrolusite content (shown in the inset of Fig. 1) corresponding to a particular structural arrangement. This begins at $P_r = 0.65$ for 2 mA g^{-1} and shifts towards slightly more pyrolusitic structures for higher rates. Structures either side of this, i.e., more ramsdellite-like structures and highly pyrolusitic materials, are less conducive to good performance. This finding confirms that the crystallites of HEMD are multi-phase, as reported previously [11]. While the role of the phase boundaries and other structural defects in the mechanism of lithium diffusion in HEMD is currently unknown, at this stage it is evident that these defects play an important part in improving the electrochemical performance of HEMD in lithium batteries.

It is interesting to compare our results with those reported by Balachandran et al. [12], who used first principles computations to examine proton diffusion through ramsdellite and pyrolusite. Their work demonstrated that protons diffuse through ramsdellite with a lower activation energy barrier than pyrolusite (∼200 meV versus 575 meV, respectively). Their model does not reveal how increments of P_r influence the ease of diffusion. While activation energies for lithium ion transport have not been determined using this analysis method, we have demonstrated that neither a ramsdellite nor pyrolusite structure is optimal, but rather a given fraction of both, depending on discharge rate.
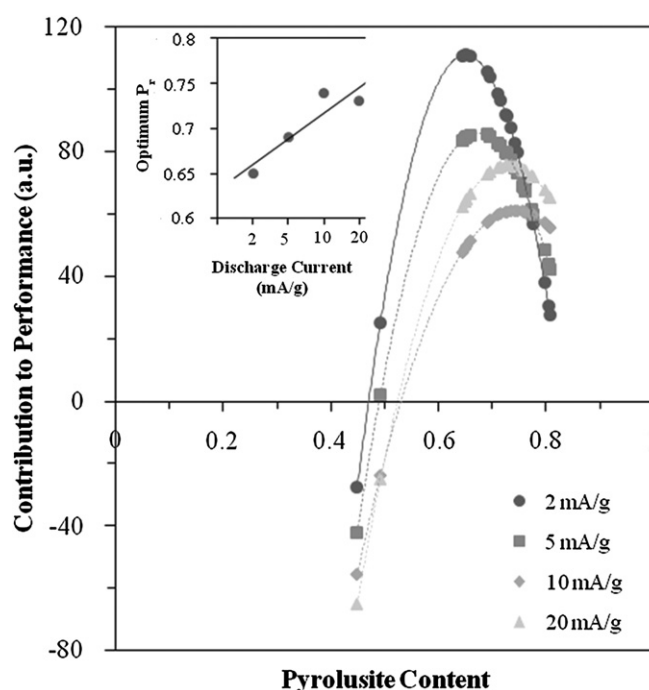
Fig. 1. Influence of the pyrolusite content on electrochemical performance. The inset shows the optimum pyrolusite content at the four discharge rates.
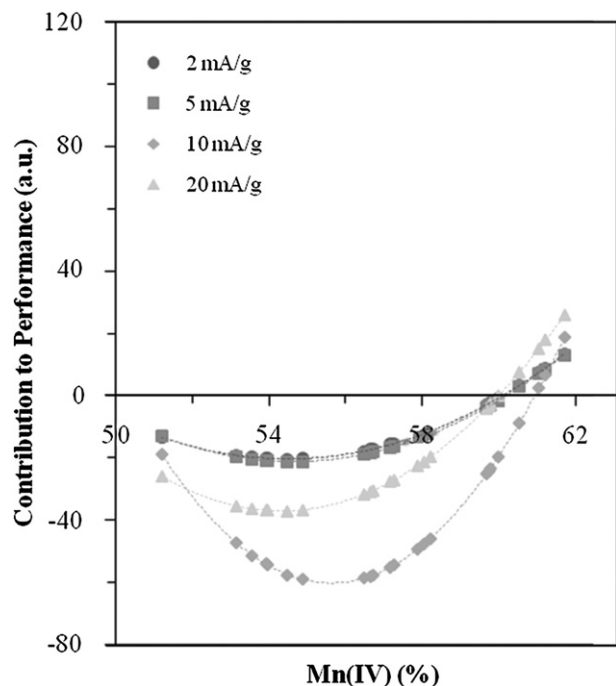
Fig. 2. Effect of the percentage of Mn(IV) on electrochemical performance.

The effect of Mn(IV) percentage within HEMD on the electrochemical performance (Fig. 2) indicates that, as expected, higher proportions of this species contribute more to higher capacity. However, materials with below 60% Mn(IV), irrespective of discharge rate, show a negative contribution to performance. This arises because of the inversely proportional relationship between Mn(IV) and Mn(III); a low Mn(IV) implies high Mn(III), which acts to reduce the specific capacity of the material.

Fig. 3 demonstrates that BET surface areas in the range examined have a detrimental effect on electrochemical performance under low discharge rates, but become more beneficial at higher rates. Further, at low discharge rates, both low and high surface area
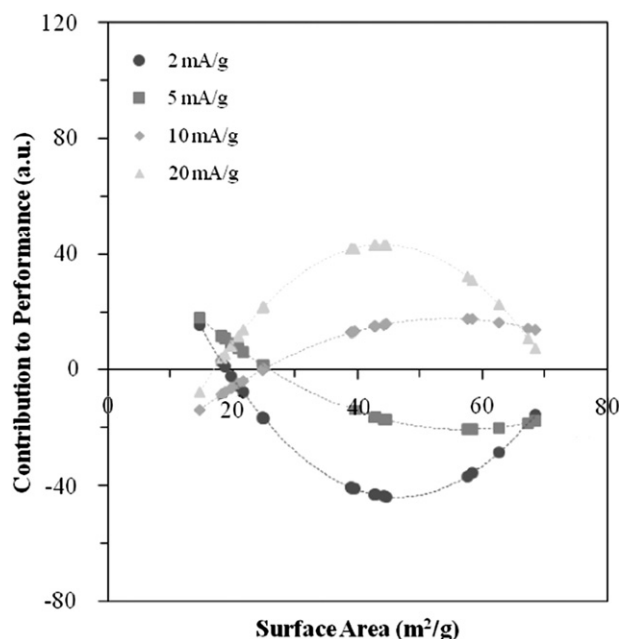

Fig. 3. Influence of the BET surface area on electrochemical performance.

materials are less damaging to the capacity, and are therefore more desirable. The opposite is true at the higher rates, where these materials contribute less to good performance.

The negative contribution to performance at lower discharge rates may result from a phase change at the surface in response to lithiation intercalation, evidence for which has been reported in our earlier study on the reduction mechanism of HEMD [13]. While this transformation is yet to be characterized in greater detail, the slow lithium ion penetration at low discharge rates may result in only a small fraction of the particle being accessed before lithium residing in the surface regions causes a phase change. If the diffusion of lithium ions is slower through this layer and/or it is less conductive, it would render the remaining core of the particle less accessible to lithiation and hence limit full utilization.

A less negative contribution for materials with high surface area can be attributed to the higher volume of micropores (those <2 nm wide) which increase significantly for materials with higher porosity. At low rates, lithium movement along these pores may be possible, hence allowing more of the active material to be utilized. Conversely, for a low surface area material a lower proportion of the surface layer may be formed, which is therefore less destructive to performance.

For high rate discharge, materials in the range of surface areas considered contribute in a positive way to performance. Discharge at these rates would be affected later by the surface phase formation, since the lithium ions are inserted faster, and consequently more of the material may be accessed before the surface layer becomes limiting. However, a low surface area is of less benefit to performance since the exposure of the manganese dioxide surface to lithium ion intercalation is limited. Consequently, inserted lithium ions must diffuse along a longer path through the solid state to access the core of particles. As lithium ions are driven into the structure the long diffusion path length and slow solid state kinetics become severely limiting, leading to poorer utilization. A highly porous material also acts to limit the capacity at high rates. The higher number and/or longer network of micropores which lead to high porosity may limit the diffusion of the lithium ion, or simply be too small to allow diffusion along them. While the movement of lithium along these pores may be adequately fast for low discharge rates, at high rates these kinetic limitations become detrimental to electrochemical performance. We reported previously that water removal from highly porous EMD is retarded, possibly due to slower H$^+$ diffusion through the extensive, heavily microporous network [8]. It follows that the diffusion of the larger lithium ion experiences similar limitations, but to a greater degree, in the discharge process of these batteries. Together, the limitations of low and high surface area materials result in an optimum surface area for the 20 mA g^{-1} discharge rate, found to be 44 m^2 g^{-1}.

4. Summary and conclusions

The electrochemical performance of HEMD in lithium batteries has been related to the numerous properties which characterize the material. In doing this, some materials exhibiting superior performance in terms of specific energy with comparable specific power to those previously reported in the literature [14] have been synthesized, with further improvements anticipated through intelligent design of materials applying the relationships outlined in this study.

References

[1] D. Linden, T.B. Reddy, Handbook of Batteries, third ed., McGraw-Hill, New York, 2002.

[2] C.S. Johnson, J. Power Sources 165 (2007) 559.

[3] H. Ikeda, T. Sauto, H. Tamura, in: Proc. MnO_2 Symp., vol. 1, 1975, p. 384.

[4] Y. Shao-Horn, S.A. Hackney, B.C. Cornilsen, J. Electrochem. Soc. 144 (1997) 3147.

[5] W. Bowden, C. Grey, S. Hackney, X.Q. Yang, Y. Paik, F. Wang, T. Richards, R. Sirotina, ITE Lett. Batt. New Technol. Med. 3 (2002) B1.

[6] W.M. Dose, S.W. Donne, J. Electrochem. Soc. 158 (2011) A1036..

[7] W.M. Dose, S.W. Donne, J. Therm. Anal. Calorim. 105 (2011) 113.

[8] W.M. Dose, S.W. Donne, Mat. Sci. Eng. B 176 (2011) 1169.

[9] R.P. Williams, Characterisation and Production of High Performance Electrolytic Manganese Dioxide for Use in Primary Alkaline Cells, Ph.D. thesis, University of Newcastle, Australia, 1995.

[10] B.D. Desai, J.B. Fernandes, V.N.K. Dalal, J. Power Sources 16 (1985) 1.

[11] S. Turner, P.R. Buseck, Nature 304 (1983) 143.

[12] D. Balachandran, D. Morgan, G. Ceder, J. Solid State Chem. 166 (2002) 91.

[13] W.M. Dose, J. Lehr, S.W. Donne, Mat. Res. Bull. 47 (2012) 1827.

[14] P. Simon, Y. Gogotsi, Nat. Mater. 7 (2008) 845.